2015

Spatial and temporal variation in penetrative strain during compression: Insights from analog models

Caroline M. Burberry
University of Nebraska-Lincoln, cburberry2@unl.edu

Published in *Lithosphere* 7:6 (2015), pp 611–624. doi:10.1130/L454.1

Submitted 7 March 2015; revised 7 July 2015; accepted 23 July 2015; published online 24 August 2015.

Spatial and temporal variation in penetrative strain during compression: Insights from analog models

Caroline M. Burberry

Department of Earth and Atmospheric Sciences
University of Nebraska–Lincoln, Lincoln, Nebraska 68588, USA

Abstract

Penetrative strain constitutes the proportion of the total shortening across an orogen that is not accommodated by the development of macroscale structures such as folds and thrusts. The accommodation of shortening by penetrative strain is widely considered to be an important process during compression, but variation in the distribution of penetrative strain during a deformation sequence is not well understood. This study provides some first-order constraints on magnitude, timing, and distribution of penetrative strain during deformation. Eight simple models, each with a geometrically and mechanically similar starting configuration, within the limits of sandbox models, were shortened to different amounts. Model results indicate first that penetrative strain increases with depth in any given model, and second that the proportion of the total shortening accommodated by penetrative strain varies with time. As the deforming wedge approaches stability, penetrative strain is highest just before initiation of a new thrust fault, after which the penetrative strain component abruptly decreases. Each model also contains a foreland zone of penetrative strain, in which penetrative strain decreases exponentially away from the deformation front. These results are consistent with available field data. Restoration of a seismic-scale cross section indicates that model results can be used to predict the amount of penetrative strain and thus the true total shortening across a deformed region. Estimates of this type may be made for additional cross sections and may provide answers to the problem of "missing shortening" across orogens and the total amount of shortening experienced at collisional plate margins.

Introduction

Penetrative strain constitutes the proportion of the total shortening across an orogen that is not accommodated by the development of macroscale structures such as folds and thrusts. Penetrative strain can include layer-parallel strain (defined strictly as the maximum contractional strain accumulated parallel to layering; Groshong, 1975), and later strains that are imposed horizontally on layers that are no longer horizontal (Couzens et al., 1993; Mitra and Yonkee, 1985). On the grain scale, penetrative strain may be accommodated by a combination of intragranular deformation such as twinning, dislocation glide and creep, or the development of other strain fabrics, and intergranular processes such as stylolitization, cleavage development, or grain impingement (Groshong, 1975; Engelder and Engelder, 1977; Engelder, 1979; Henderson et al., 1986; Onasch, 1993; Tavarnelli, 1997). On a larger scale, slip on arrays of minor faults and the development of systematic minor fold sets may also accommodate penetrative strain when considered across the scale of a regional cross section (Wojtal, 1989; Hogan and Dunne, 2001).

Accommodation of shortening by penetrative strain is widely considered to be an important process during compression of the continental lithosphere, on a variety of time and length scales. This process may be a significant in reconciling the discrepancy between observed shortening rates and inferred geologic shortening rates and amounts ("missing shortening") across orogens, for example, across the India-Asia collisional margin (Johnson, 2002). Estimates of shortening are typically given as minima, and they may consist of large ranges or rest on the assumption that shortening rates are constant over millions of years (e.g., Agard et al., 2005; Guest et al., 2006). Additional methods of reconciling the discrepancy are to invoke significant strike-slip motion and lateral extrusion of material (e.g., Guillot et al., 2003) or to invoke additional microplates in the deforming system and thus strain partitioning between numerous boundaries (Nilforoushan et al., 2003; Vernant et al., 2010; Mouthereau et al., 2012), with variable shortening rates on individual

boundaries. Underthrusting of crustal material and the detachment of the sedimentary section from the downgoing plate are also invoked to explain the discrepancy (Zhao et al., 1993). The variation in shortening rate as deduced from global positioning system (GPS) data may also imply extension along the strike of the orogen (Hessami et al., 2006), indicating that geologic models that only consider shortening by folding and thrusting may be oversimplified.

Deformation of a thrust sheet can be described in terms of a bulk translation, a bulk rotation, and an amount of internal strain (e.g., Mitra, 1994; Yonkee and Weil, 2010; Sussman et al., 2012). An underestimate of any of these components leads to an underestimate of the total shortening. All thrust sheets undergo a bulk translation, which can be approximated by reuniting hanging-wall and footwall cutoffs. All thrust sheets also undergo a verticalaxis rotation, which is most pronounced in regions of the thrust sheets where the transport direction is divergent (Kwon and Mitra, 2004; Sussman et al., 2012). Thus, in regions of divergent rather than uniform transport direction, neglecting vertical-axis rotation may introduce as much error into shortening estimates as neglecting penetrative strain.

Considering the penetrative strain aspect of this problem, incorporating penetrative strain correctly into restorations of crustal-scale deformation requires an understanding of how strain measurements taken across a deformed region relate to the development of penetrative strain throughout deformation and the cumulative amount of penetrative strain accommodated during shortening. The amount of penetrative strain is variable in time and space (e.g., Beutner and Charles, 1985; Groshong and Epard, 1994; Mitra, 1994; Epard and Groshong, 1995; Koyi, 1995; Weil and Yonkee, 2009). Mitra (1994) showed that the internal strain within thrust sheets is inhomogeneous, increasing from the front to the back of the thrust sheet, and it is independent of the translation of the sheet. Mitra (1994) further showed that internal strains in the frontal thrust sheets are smaller than the internal strains in the hinterland thrust sheets. Typically, the development of penetrative strain–related features is considered to be a process that occurs early in the deformation process, before the development of macroscale structures (e.g., Geiser and Engelder, 1983; Mitra and Yonkee, 1985; Wiltschko et al., 1985; Henderson et al., 1986; Dean et al., 1988; Tavarnelli, 1997; Whitaker and Bartholomew, 1999; Weil and Yonkee, 2009), sometimes with a relationship to the developing thrust ramp (Fischer and Coward, 1982). Some authors have recognized multiple potential episodes of layer-parallel shortening (Geiser and Engelder, 1983; Gray and Mitra, 1993). The observation of these distinct episodes of penetrative strain development may be a function of the anisotropy in natural layered sequences, which are strongest when the applied stress is either subhorizontal or subperpendicular to the layering (Fisher, 1990), suggesting that discrete structures formed by penetrative strain may only be recorded when the layering is strongest. In addition, Tapp and Wickham (1987) showed that the incremental strain axes in episodes of penetrative strain development are not always coaxial or parallel to bedding. The strain axes for the accumulated penetrative strain were found to be a reasonable approximation to the incremental strain axes, however (Tapp and Wickham, 1987). The amount of penetrative strain accommodated in a given region is also affected by variations in lithology of the overburden, the presence and specific rheology of any detachment layers, and the dip of the base of the deforming wedge, as well as the relative location within the orogen (Mitra, 1994; Whitaker and Bartholomew, 1999; Couzens-Schultz et al., 2003; Koyi and Vendeville, 2003; Sans et al., 2003; Koyi et al., 2004; Nilforoushan and Koyi, 2007; Weil and Yonkee, 2009). Penetrative strain features can be found up to 1200 km from the active plate margin (Craddock and van der Pluijm, 1989).

Measured amounts of penetrative strain range from 2% to 30%, where the larger end of this range may form a significant component of the total shortening (Engelder and Engelder, 1977; Engelder, 1979; Mitra and Yonkee, 1985; Wiltschko et al., 1985; Craddock and van der Pluijm, 1989; Mitra, 1994; Whitaker and Bartholomew, 1999; Sans et al., 2003; Koyi et al., 2004; Weil and Yonkee, 2009). Penetrative strain amount appears to decay away from the developing thrust front (Craddock and van der Pluijm, 1989; Koyi, 1995). Different mechanisms (intravs. intergranular) may record different amounts of penetrative strain in a system; thus, the total penetrative strain must be estimated as a sum of components occurring in any given unit or thrust sheet (Groshong, 1975; Engelder, 1979; Mitra and Yonkee, 1985; Wiltschko et al., 1985; Mitra, 1994; Hogan and Dunne, 2001; Sans et al., 2003).

The studies cited herein report significant variation in the amount and distribution of penetrative strain within a deforming system, but few papers focus on systematically quantifying and characterizing the distribution and temporal evolution of penetrative strain features and the amount of penetrative strain accommodated in different parts of the deforming system. An exception to this statement is the growing body of work on the Wyoming salient, a Sevier-age foldand- thrust belt, which deformed as a progressive arc, with rotation of early penetrative strain fabrics (Mitra et al., 1984; Weil and Yonkee, 2009; Weil et al., 2010). Minor extension has also been noted along the strike of the belt (Weil et al., 2010; Yonkee and

Weil, 2010). Estimates of penetrative strain within this belt range from <5% in red beds in the frontal part of the salient to >15% in red beds in interior systems and the curved salient ends (Weil and Yonkee, 2009). Mitra (1994) reported penetrative strains of ~30% in the cover of the internal thrust sheets, a result echoed by Yonkee and Weil (2010). It should be noted that these studies discussed the amount of penetrative strain in individual thrust systems, where this study considers the total amount of penetrative strain accumulated by a fold-and-thrust belt.

Thus, the purpose of this contribution is to systematically examine the effect of increased shortening on the total amount and two-dimensional (2-D) distribution of penetrative strain, within a very simple mechanical system. The models will be compared to the Wyoming salient example, in order to provide some constraints on the amount of "missing" shortening across natural systems. A series of mechanically simple models with similar starting configurations were shortened by variable amounts, and penetrative strain was assessed throughout the deformation sequences, thereby allowing an evaluation of the amount of layer-parallel strain and the extent to which it varied in space throughout the deformation sequence. It is important to remember that the mechanisms of penetrative strain accommodation in nature and models are different; the strain in the models is taken up by grain-grain displacement only, rather than the mechanisms detailed earlier herein. Thus, the models can only establish some first-order constraints on (1) the timing of penetrative strain–related structure formation, (2) the amount of penetrative strain accommodated throughout deformation stages, and (3) the distribution of penetrative strain in the deforming system throughout the deformation sequence.

Materials and Methods

In this study, the behavior of a brittle sand pack was modeled using a purpose-built experimental setup (Fig. 1). This consists of a box with one moving wall driven by a stepper motor, and two cameras set up and leveled to photograph the top surface of the model and the side view (Fig. 1A). The modeling apparatus was 48 cm wide, and in these experiments, it had an initial starting length of 64 cm. The base, moving wall, and fixed wall were made of waterproofed plywood, and the side walls were made of glass. This results in a model with a relatively high basal friction. Side walls were not lubricated during experimental runs, as the model apparatus was sufficiently wide to obtain results in the center of the apparatus that were free from edge effects. An empirical rule for avoiding the section of the model affected by edge effects is to avoid a margin equal to or greater than the height of the sedimentary wedge. Typically, representative sections are sliced between 8 and 40 cm from one side wall, thus leaving a margin of 8 cm that contains areas of the model affected by edge effects, and 32 cm that can be reasonably used for analysis (Fig. 1B). The stepper motor, which drives the moving wall, is capable of driving the wall at a constant rate of between 4 and 16 mm/h. Typical model runs used a driving rate of 8 mm/h. The apparatus was allowed to dry out between experiments and was thoroughly cleaned.

Eight analog models were run to investigate the overall amount of penetrative strain accommodated by a deforming thrust system, and to constrain the amount and distribution of this penetrative strain through the wedge and foreland over successive increments of deformation. Each model consisted of four 5-mm-thick layers of fine quartz sand poured into the deformation apparatus and smoothed using a scraper, but not compacted (Fig. 2). The sand was sifted before use, to remove grains larger than the desired grain size. A standard test sieve (#35) was used; thus, the material used in experiments had a grain size of less than 0.5 mm. Marker layers made of dyed fine quartz sand were used to separate the layers and were used as key units to assess shortening. A grid was imprinted on the top surface of each model in order to track strain patterns in the foreland in successive shortening increments. Each model had the same starting length (640 mm; Fig. 2); thus, the initial setup of all models was similar. No along-strike variation was introduced into the models, so, as far as possible, the starting configuration of all models was similar. Models 1–8 were shortened by different amounts, with model 1 shortened by the smallest amount and model 8 shortened by the greatest amount (Table 1).

Table 1. List of All Models Considered in This Study, with Their Respective Shortenings

Model	Displacement of back wall (mm)	% shortening
1	13	4.3
2	32	10.7
3	45	14.9
4	64	21.3
5	77	25.6
6	96	32.0
7	109	36.3
8	128	42.7

Shortening is shown both as a displacement of the back wall and % total shortening with respect to the constant pin line placed 300 mm from the initial position of the back wall (original length for calculation purposes, 300 mm).

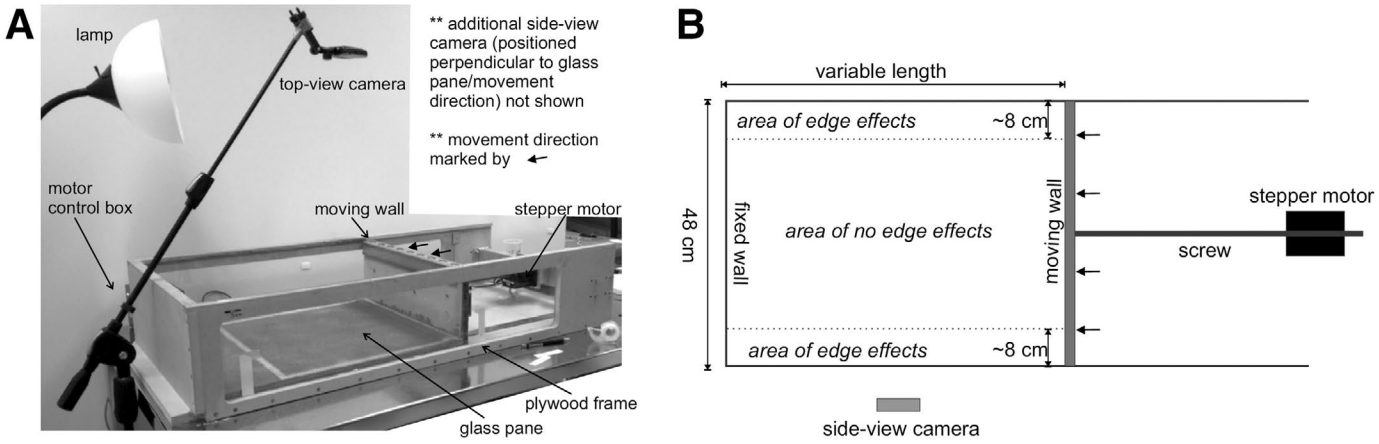

Figure 1. Modeling apparatus used in this study. (A) Labeled oblique-view photograph of modeling apparatus, with an experiment running. (B) Planview diagram of the apparatus showing the areas where edge effects are present and the area used for analysis in the center of the model.

Since this model series was designed to be a simple system for the purposes of setting constraints on penetrative strain timing, magnitude, and distribution, the models were not scaled to match any specific natural situation. However, the fine colored quartz sand used for the marker layers and the undyed fine quartz sand used for the bulk of the model were mechanically similar, both having coefficients of internal friction of 0.59 (angle of internal friction 30.5°). This measurement was made in the laboratory after Krantz (1991) using a modified Hubbert apparatus (Hubbert, 1937). The same materials were used for all models, and so models were mechanically similar. Finally, all models were dynamically similar, since material density, shortening rate, and initial geometry were not varied (Koyi, 1997).

Fine, rounded quartz sand is typically used to represent brittle sedimentary units in scaled analog models (Moretti and Callot, 2012). The sand shows limited elastic deformation at the stresses imposed in these analog experiments, rather deforming by strain hardening (that is, compaction of the grains to remove pore space generated during model setup) followed by failure (the generation of faults) and strain softening until a stable dynamic strength is reached (Lohrmann et al., 2003; Ellis et al., 2004; Panien et al., 2006; Buiter, 2012). This behavior is found to resemble the stress-strain curves generated in standard compression tests of rocks (Li et al., 1998; Jaeger et al., 2007) and indicates macroscopic similarity between sandbox and upper-crustal mechanics. The behavior of the sand at laboratory-scale normal stresses is best described using the relationship between cohesion and normal stress, rather than angle of internal friction and normal stress (Schellart, 2000). Rounded sand grains are preferred in analog experiments because the cohesion and angle of internal friction values scale more accurately to those of real brittle rocks.

During shortening, photographs were taken of the top surface and side view of each model. Photographs were taken at every ~6 mm shortening increment, as well as of the initial and final configurations. Side-view photographs were used to calculate the surface slope (Fig. 3A), which did not vary appreciably from model center to the edge, despite the rotation caused by edge effects. Top surface photographs were used to track the appearance of new thrust sheets. Top surface photographs, showing the developing wedge and the deforming surface grid, were also used to (1) measure the average width of the deforming wedge, measured from frontal thrust to the back wall

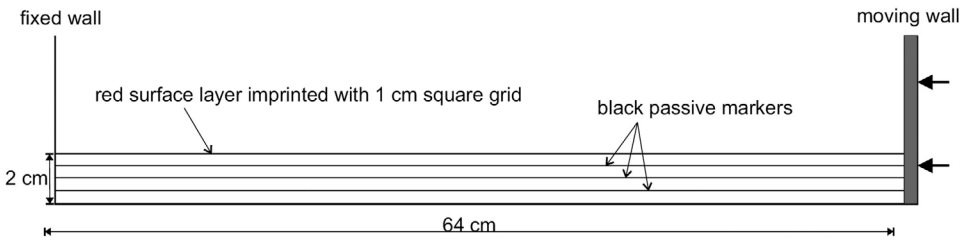

Figure 2. Diagram of initial model configuration used in this study, with dimensions.

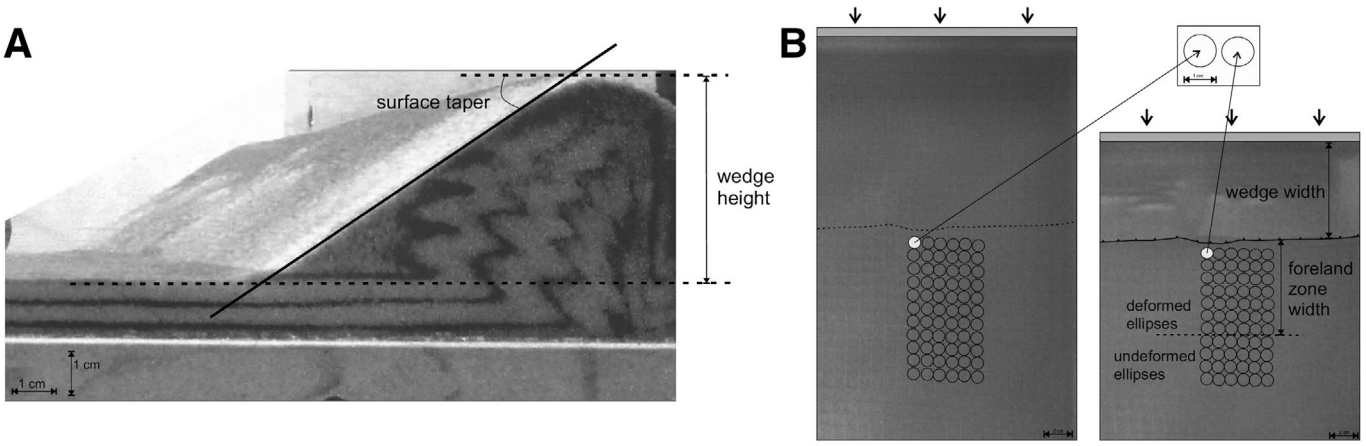

Figure 3. Measurements taken as part of model analysis. (A) Side-view photograph labeled with surface taper and wedge height measurements. (B) Plan-view photograph showing initial and deformed grid states fitted with strain ellipses, together with measurements of wedge and foreland deformation zone width.

of the apparatus, (2) track the amount of strain accommodated in the foreland zone, and (3) measure the width of the foreland deformation zone, ahead of the frontal thrust sheet. Unit circles were fitted to the undeformed grid, and strain ellipses were fitted to the deformed grid (Fig. 3B). The amount of strain, e (Engineers extension or extension), was calculated for each part of the deformed grid using the standard formula $e = (l - l_0)/l_0$ (l—deformed length and l_0—original length), so the strain in the foreland could be quantified and the width of the deformed foreland zone could be measured.

Once each model had been shortened to the desired amount (Table 1), a sand pack was added to preserve the topography, and the model was wetted with a soap solution and sliced into cross sections. When the soap solution was introduced slowly via syringe and light spray at the edges of the model and the top of the sand pack, the liquid did not affect the configuration of the sand grains as seen in side view. Slices were made using a flat-bladed knife, and with practice, clean cuts could be made that did not distort the structure of the models. Photographs were taken of every cross section. Representative cross sections of each model were digitized using MOVE (Midland Valley software) and were restored to the original flat-layer configuration using both unfolding and unfaulting algorithms (Fig. 4). Thrusts were restored sequentially, in reverse order of formation, thus restoring the youngest thrust first. Each step of restoration involved reuniting the hanging-wall and footwall cutoffs of the layers (unfaulting) and then removing the associated folding using the unfolding algorithm. The only assumption made was that of plane strain, which is reasonable since the model setup did not allow for significant out-of-plane movement in the central portion of the model. The only significant rotation occurred in the edge regions, which were purposely excluded. From these restored cross sections, the amount of shortening accommodated by folding and thrusting was calculated. The discrepancy between the calculated tectonic shortening and the known total shorten ing represents the shortening accommodated by penetrative strain. Volume loss by sand escape was negligible in these models, as the moving wall was a snug fit to both the base and sides of the shortening apparatus, and so the discrepancy between total shortening and calculated tectonic shortening can be reasonably assumed to be from penetrative strain. There was also minimal sand escape and unroofing of deeper layers at the top of the wedge.

In these experiments, the penetrative strain component of the deformation was taken up entirely by compaction of grains to remove pore space generated during model setup. This compaction introduced a component of strain hardening into each thrust sheet, and it indicates that the region of most penetrative strain accommodation must change during deformation. Most penetrative strain will be accommodated in, or in front of, and below the active thrust sheet, rather than in the remainder of the wedge, implying a natural forelandward progression of the zone of maximum penetrative strain. This scenario is a simplification for several reasons. One is that in the models, penetrative strain is accommodated by one mechanism (compaction of sand grains), and in nature, penetrative strain may occur by a number of different mechanisms, including calcite twinning and pressure solution, as noted previously. In addition, penetrative strain in nature can often be separated into an earlier, typically layer-parallel strain, and a later stage of penetrative strain, which will not necessarily be layer-parallel due to layer rotation (Geiser and Engelder, 1983; Couzens et al., 1993; Gray and

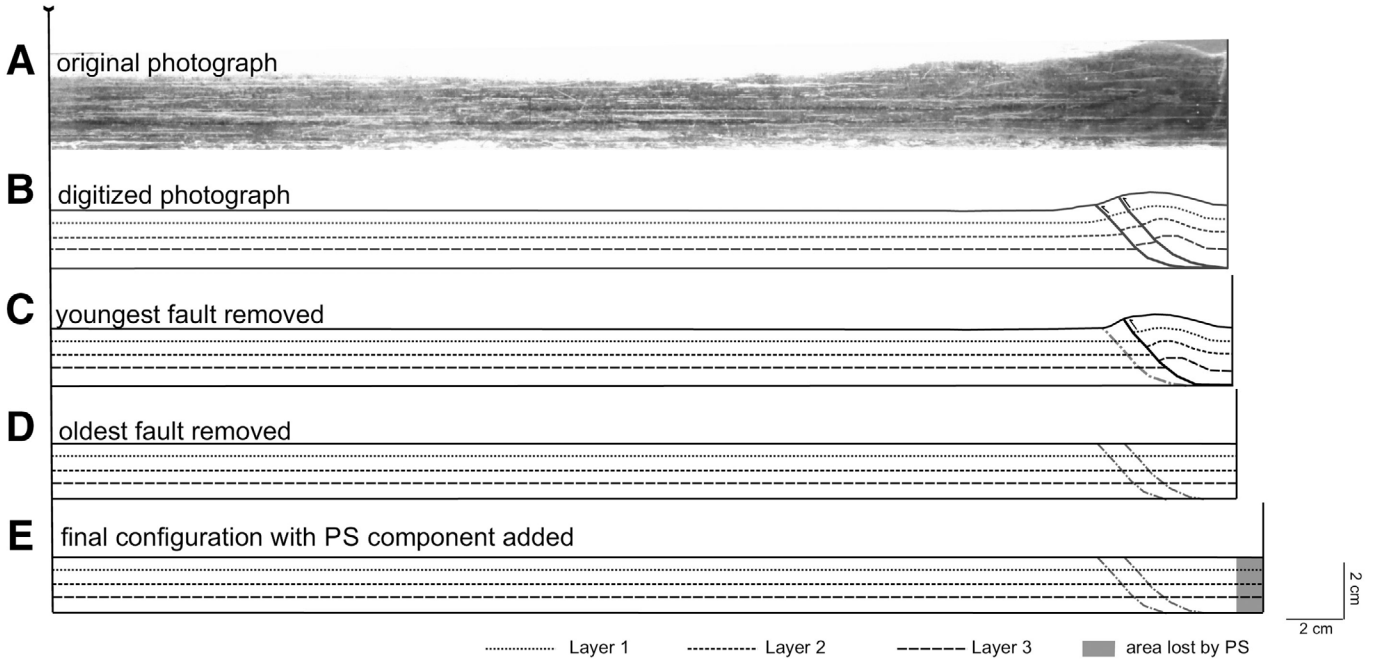

Figure 4. Stages in stepwise restoration of cross sections. (A) Initial photograph from model 1. (B) Digitized line drawing of the photograph in A. (C) Line drawing of the section once the displacement and folding associated with the youngest fault have been removed. (D) Line drawing of the section once the displacement and folding associated with the next fault have been removed. (E) Final restored configuration including the amount of shortening accommodated by penetrative strain (PS, gray shading).

Mitra, 1993). These distinct events do not appear to occur in the models, perhaps because the sand pack is not sufficiently anisotropic, even under variable shortening directions. Thus, penetrative strain deduced from these models is probably an underestimation of the natural strain magnitudes that might occur if other mechanisms were present. However, given the variation in the amounts and locations of penetrative strain reported from nature, summarized earlier herein, these models are considered to provide valuable first-order constraints on penetrative strain distribution during deformation.

Results

Each model deformed by the development of piggyback thrusts and associated fault-propagation folds, forming a sand wedge that increased in height and width as shortening progressed. Figures 5–8 show photographs and line drawings of representative cross-section slices from successive models. Each successive model underwent increasing shortening, and so the number of thrusts developed in each model and the size of the deforming wedge increase from one model to the next. Shortening amounts here are given assuming an initial length of 30 cm for each model. This removes the 34 cm of model that was not deformed in any experiment from the calculations and gives realistic shortening percentages for comparison to natural examples.

At first glance, wedge height and width appear to grow steadily, although the increase in width is slightly greater in shortening increments where a new thrust is developing (Fig. 9). However, when the increments of width or height increase in each stage are considered, together with the variation in surface slope, wedge growth can be divided into three distinct phases of deformation (Fig. 10). Phase 1, covering the range of ~2%–15% total shortening, is characterized by an overall decrease in height growth increments, and rapid jumps in both width growth increments and surface taper. Larger changes in width growth increment and surface slope correlate with the initiation of new thrusts. In this phase, the wedge has not yet reached a stable configuration. New thrusts are added at nearly every shortening increment, creating a rapidly changing developing thrust wedge. Phase 2, covering the range of 17%–30% total shortening, is characterized by relatively steady height growth increments, lower than in the previous stages, and organized oscillations in both width growth increments and surface slope. Again, the large increases in wedge width and abrupt changes in surface slope correlate to the initiation of new thrusts. Initiation of new thrusts is less rapid in this stage, creating a wedge that is tending toward stability. Phase 3,

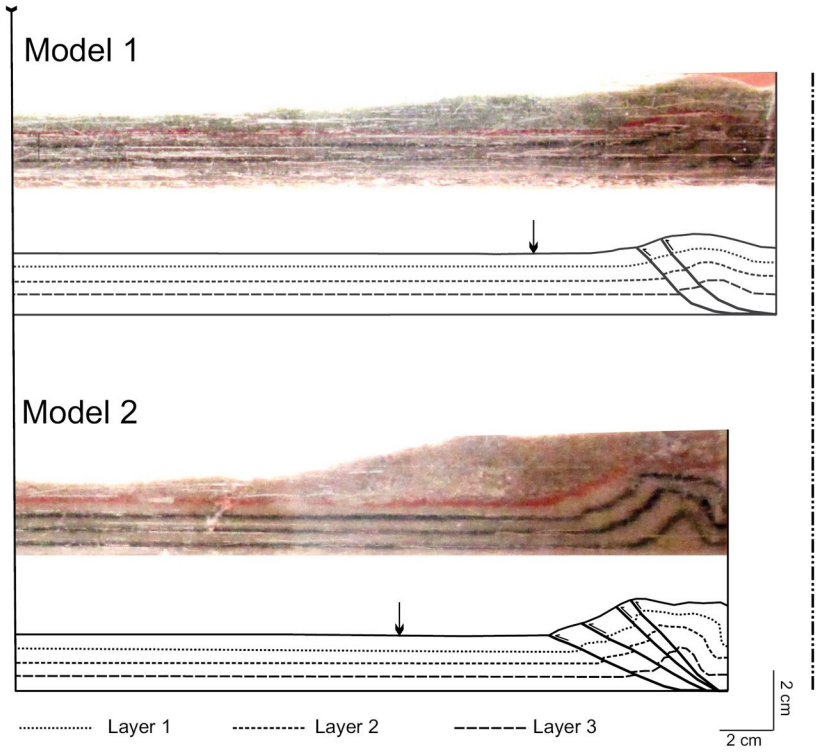

Figure 5. Representative cross sections from models 1 and 2. Both photographs and digitized line drawings are shown. The arrow marks the limit of the foreland deformation zone.

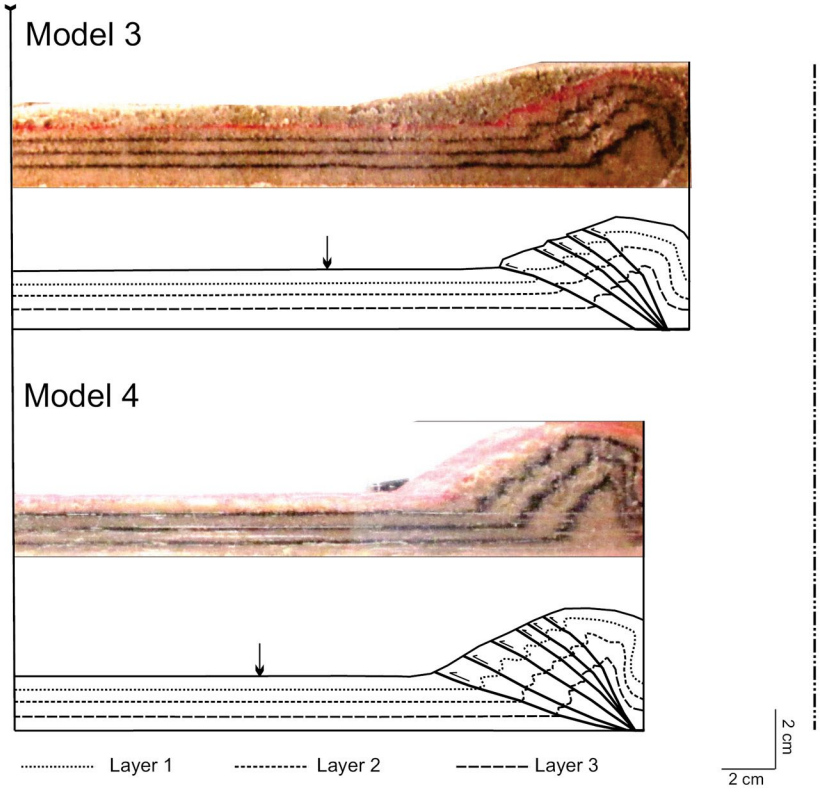

Figure 6. Representative cross sections from models 3 and 4. Both photographs and digitized line drawings are shown. The arrow marks the limit of the foreland deformation zone.

covering the range of 32%–43% total shortening, is characterized by a near-constant height growth increment, a near-constant surface slope, and a regularly oscillating width growth increment. Again, the oscillations in width growth increment correlate to the initiation of new thrusts. New thrusts initiate every 10% shortening, creating a stable wedge that deforms in a self-similar fashion, marked by a near-constant surface slope.

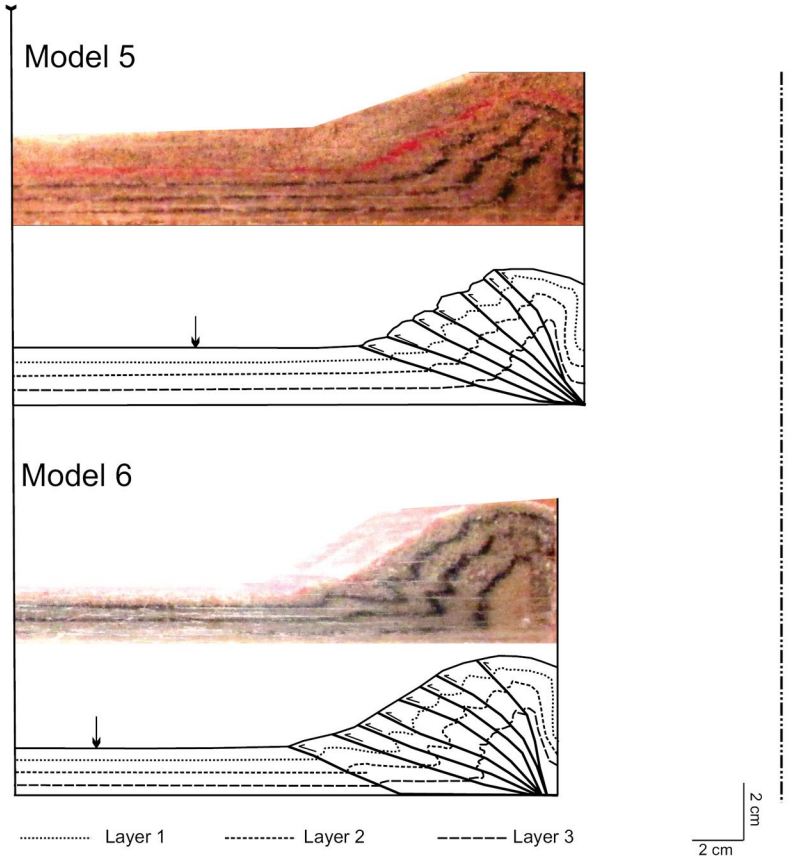

Figure 7. Representative cross sections from models 5 and 6. Both photographs and digitized line drawings are shown. The arrow marks the limit of the foreland deformation zone.

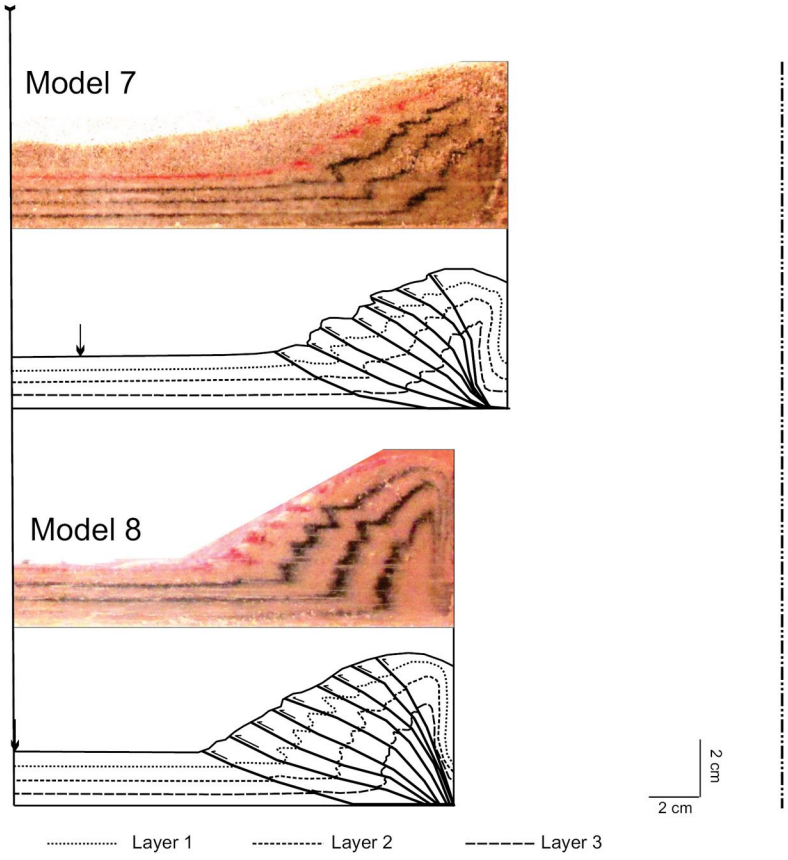

Figure 8. Representative cross sections from models 7 and 8. Both photographs and digitized line drawings are shown. The arrow marks the limit of the foreland deformation zone

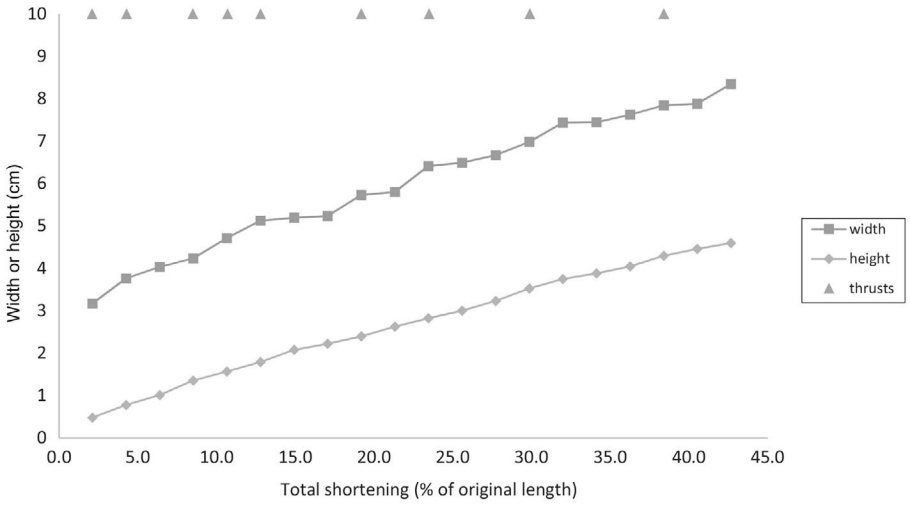

Figure 9. Progressive change in wedge width and height (measured as height above the original surface) throughout the deformation sequence. Gray triangles indicate the shortening increments in which new thrusts initiated.

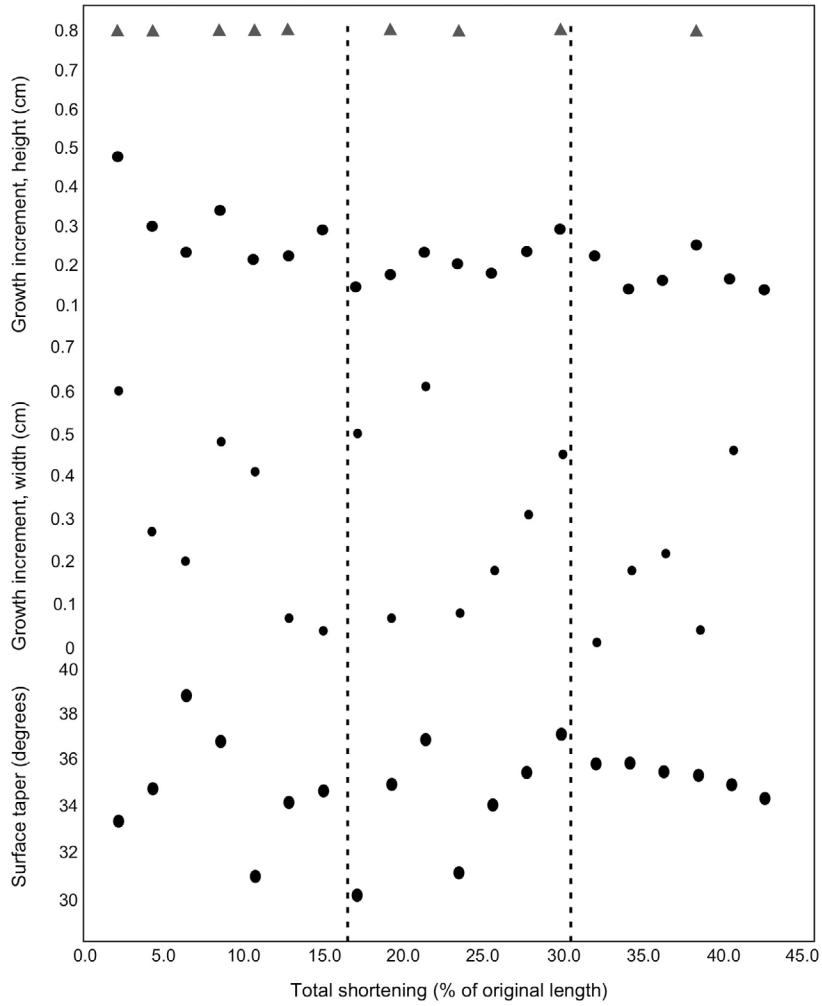

Figure 10. Detailed indices describing wedge growth: wedge height growth increment, wedge width growth increment and wedge taper. Vertical dashed lines separate the deformation sequence into three phases. Phase 1 (1%–7% shortening) represents wedge amplification, phase 2 (8%–14% shortening) represents a transitional stage, and phase 3 (15%–20% shortening) represents the stable (critical) deformation of the wedge.

Within an individual model, penetrative strain generally increases with depth. As a cor ollary to this statement, the amount of displacement on individual faults decreases with depth (Figs. 5–8). Figures 11 and 12 show restorations of the representative sections from Figures 5–8, following the workflow described and illustrated in Figure 3. The dark-gray shaded area in Figures 11 and 12 indicates the amount of shortening taken up by folding and thrusting. The pale-gray area indicates the amount of shortening that has been taken up by penetrative strain. In model 1 (Fig. 11A), the amount of penetrative strain is approximately constant with depth and is a large percentage

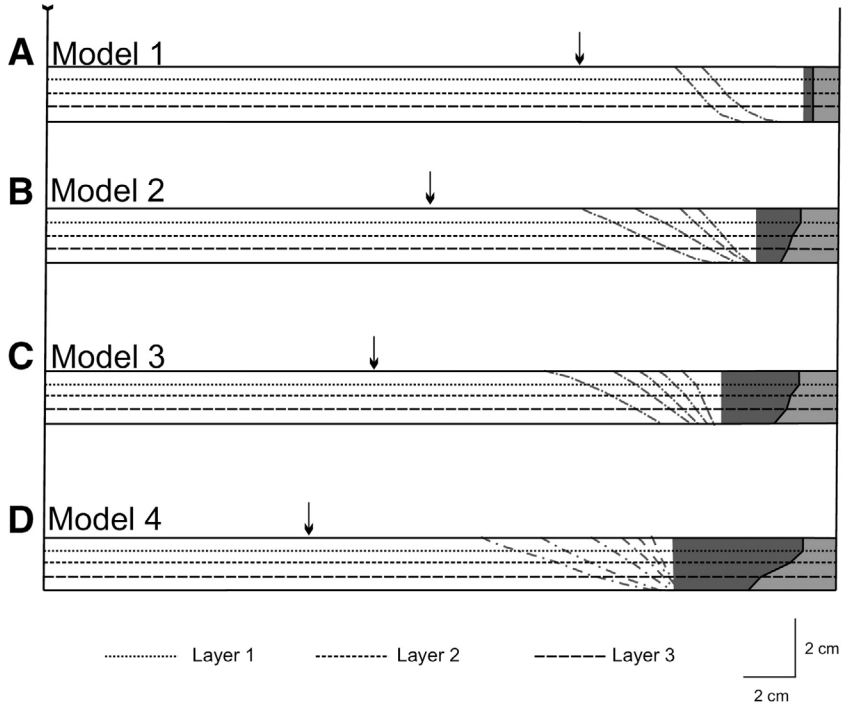

Figure 11. Restored configurations of models 1–4, including tectonic shortening (dark gray) and penetrative strain (light gray). (A) Restored configuration of model 1. (B) Restored configuration of model 2. (C) Restored configuration of model 3. (D) Restored configuration of model 4. Arrows mark the front of the foreland deformation zone.

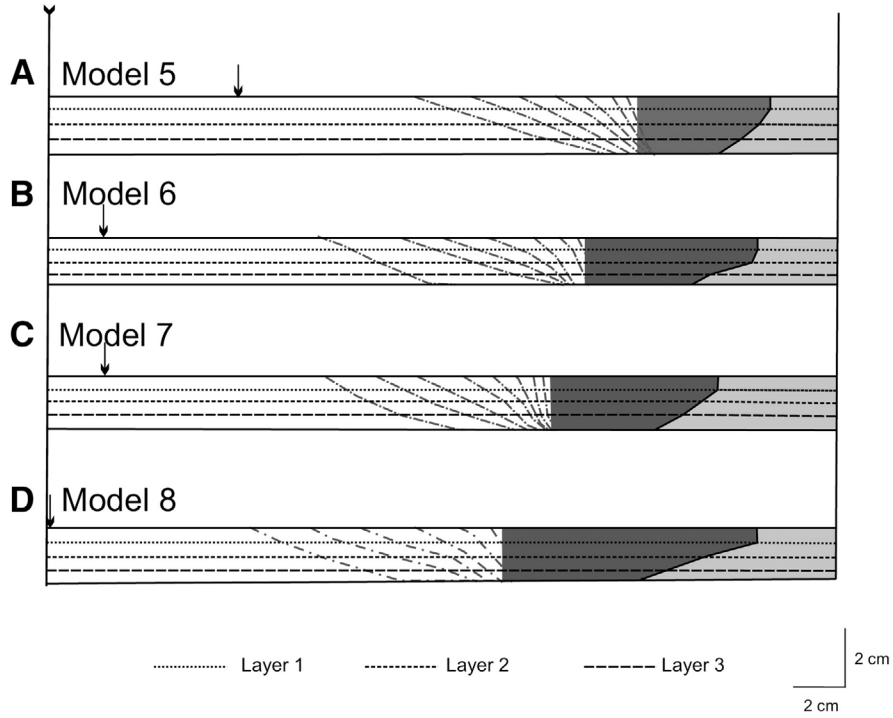

Figure 12. Restored configurations of models 5–8, including tectonic shortening (dark gray) and penetrative strain (light gray). (A) Restored configuration of model 5. (B) Restored configuration of model 6. (C) Restored configuration of model 7. (D) Restored configuration of model 8. Arrows mark the front of the foreland deformation zone.

of the total shortening. In this model, fault displacement decreases with depth, and the remaining strain is taken up by an increase in fold amplitude in the upper layers (Fig. 5A). In successive models, the amount of penetrative strain increases with depth, until model 8 (Fig. 12D), where the difference in penetrative strain amounts between layers 1 and 3 is large, as indicated by the slope of the boundary between the gray areas. Additionally, the relative contribution of penetrative strain across the whole fold-and-thrust belt as a percentage of the total shortening decreases with increasing total shortening (i.e., the contribution of folding and thrusting across the whole thrust belt increases with increasing total shortening).

This increase of penetrative strain with depth is also shown in Figure 13, where for each successive increment of shortening, layer 3 (the bottom layer; marker at 1.5 cm

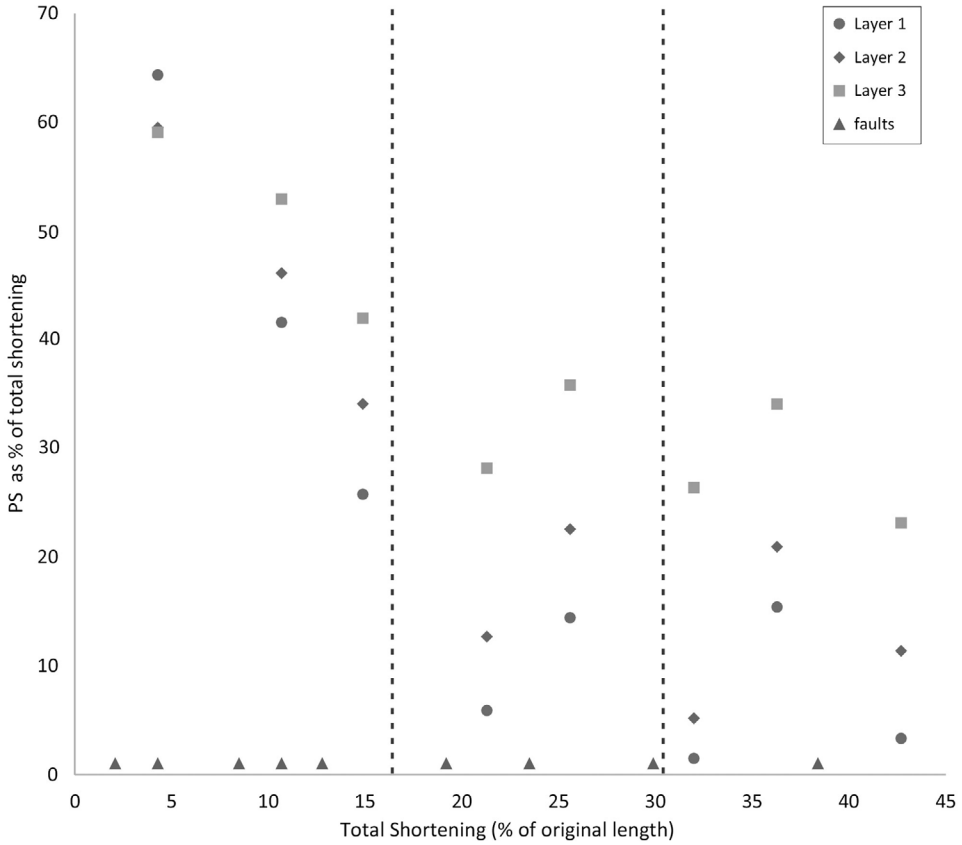

Figure 13. Variation in penetrative strain (PS) component with time. The graph is divided by vertical dashed lines into the phases noted in Figure 10 and associated text. In phase 1, the component of penetrative strain decreases in importance. In phase 2, the oscillatory nature of the penetrative strain amount with respect to thrust initiation starts to develop, and in phase 3, this oscillatory component is fully developed. Penetrative strain in phase 3 is high just before initiation of a thrust and decreases abruptly once movement has begun on that fault.

from the top of the model) has undergone more penetrative strain than either the middle layer (layer 2; marker at 1 cm from the top of the model) or the top layer (layer 1; marker at 0.5 cm from the top of the model). Figure 13 also indicates that penetrative strain is a large fraction of the total shortening in the early stages of deformation (total shortening 10.7%; model 1) and a smaller fraction of the total shortening in the later stages of deformation (total shortening 42.7%; model 8). The change in percent penetrative strain with (1) depth within an individual model and (2) the progression of deformation can also be considered in terms of the deformation phases noted earlier (Fig. 13). Phase 1, 2%–15% total shortening, is characterized by an overall decrease in the percent penetrative shortening per layer and an increasing divergence of the penetrative strain percentages for individual layers. Phases 2 and 3 are less clearly marked, but they are best considered as an oscillation in the percent penetrative strain relative to thrust initiation.

Penetrative strain is a lower percentage of the total shortening just after a thrust has initiated, and it increases up to the point when the next thrust in the sequence initiates. This is illustrated clearly between total shortening increments 12 and 18. Penetrative strain in layer 1 is ~35% of the total shortening at 25.6% total shortening (increment 12). A thrust is initiated at 29.9% total shortening, and penetrative strain in layer 1 is ~28%. By 36.3% total shortening, penetrative strain in layer 1 is ~48%, and a new thrust initiates at 38.4% total shortening. It is possible that phase 3 can be considered the behavior of the penetrative strain component in a stable wedge scenario, while phase 2, where the relationship noted between penetrative strain and thrust initiation is less clear, can be considered as a transitional phase between phase 1 (wedge initiation and development) and phase 3 (stable, self-similar wedge deformation).

In each model, a frontal thrust can be defined such that the sand pack to the foreland of this structure remains in horizontal layers and appears undeformed. However, distortion of the surface grid indicates that the foreland contains a zone of penetrative strain (Fig. 3). The foreland edge of the zone of penetrative strain is arrowed on Figures 11 and 12, as well as Figures 5–8. As the wedge grows, this zone widens and is approximately as wide as the wedge itself (Figs. 5–8 and 14). The zone of foreland strain does not grow steadily, but instead it shows three phases of growth, related to the three phases of wedge deformation. Phase 1 is marked by a rapid increase in width of the foreland deformation zone, with short periods where the zone remains the same width when new

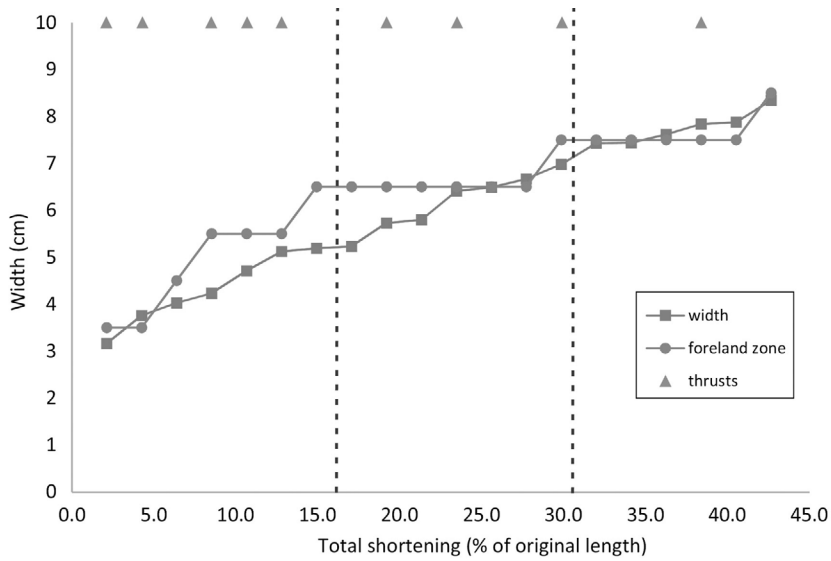

Figure 14. Variation in width of the wedge and of the foreland zone of deformation, indicating that these zones are approximately the same width. Again, vertical dashed lines indicate the three phases of deformation in these models. Phase 1 is characterized by rapid increase in width of the foreland zone, and phases 2 and 3 are characterized by this zone remaining at a constant width.

thrusts are initiating, i.e., when the bulk of the deformation is taken up by thrusting rather than by penetrative strain. There is an increase in width as phase 2 begins, but during phase 2, the width of the foreland zone of penetrative strain remains the same. The same pattern is noted at the beginning of, and during phase 3.

Within the foreland zone of penetrative strain, the amount of shortening in the final stage is highest closest to the frontal thrust of the wedge and decays exponentially away from this point, as demonstrated by the results from the final configuration of model 8 (Fig. 15). In each successive increment of shortening leading up to this point, the same overall trend is noted (Figs. 16A–16F), where at most shortening increments, there is a high penetrative strain immediately adjacent to the thrust front, with a rapidly decreasing penetrative strain away from the thrust front. No clear pattern related to thrust initiation, or deformation phases, is noted. The apparent variation in strain magnitude measured may be more of a function of the coarse measurement grid than of repeatable variation.

In summary, penetrative strain within a deforming system is found to be highly heterogeneous both in the 2-D space investigated here and over the deformation sequence. The amount of penetrative strain is found to increase with depth in any given model, no matter what stage of the deformation process. The deformation sequence has been divided into three stages: phase 1, the buildup of the wedge; phase 2, a transitional stage; and phase 3, deformation of a stable wedge. At the start of the deformation sequence, penetrative strain accommodates a large percentage of the total deformation. During phase 1, the percentage of deformation decreases. During phases 2 and 3, the contribution of penetrative strain to the overall deformation oscillates with respect to thrust initiation. Last, each model also contains a foreland zone of penetrative strain, where penetrative strain decreases exponentially within this zone with increasing distance from the frontal thrust.

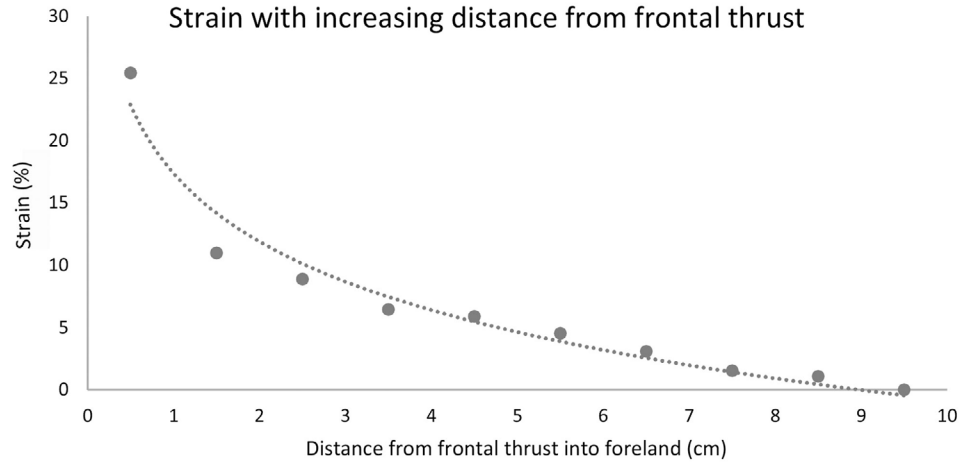

Figure 15. Data from model 8, indicating the change in penetrative strain amount recorded by the deforming grid with increasing distance from the deformation front. The data can be fitted by an exponential curve.

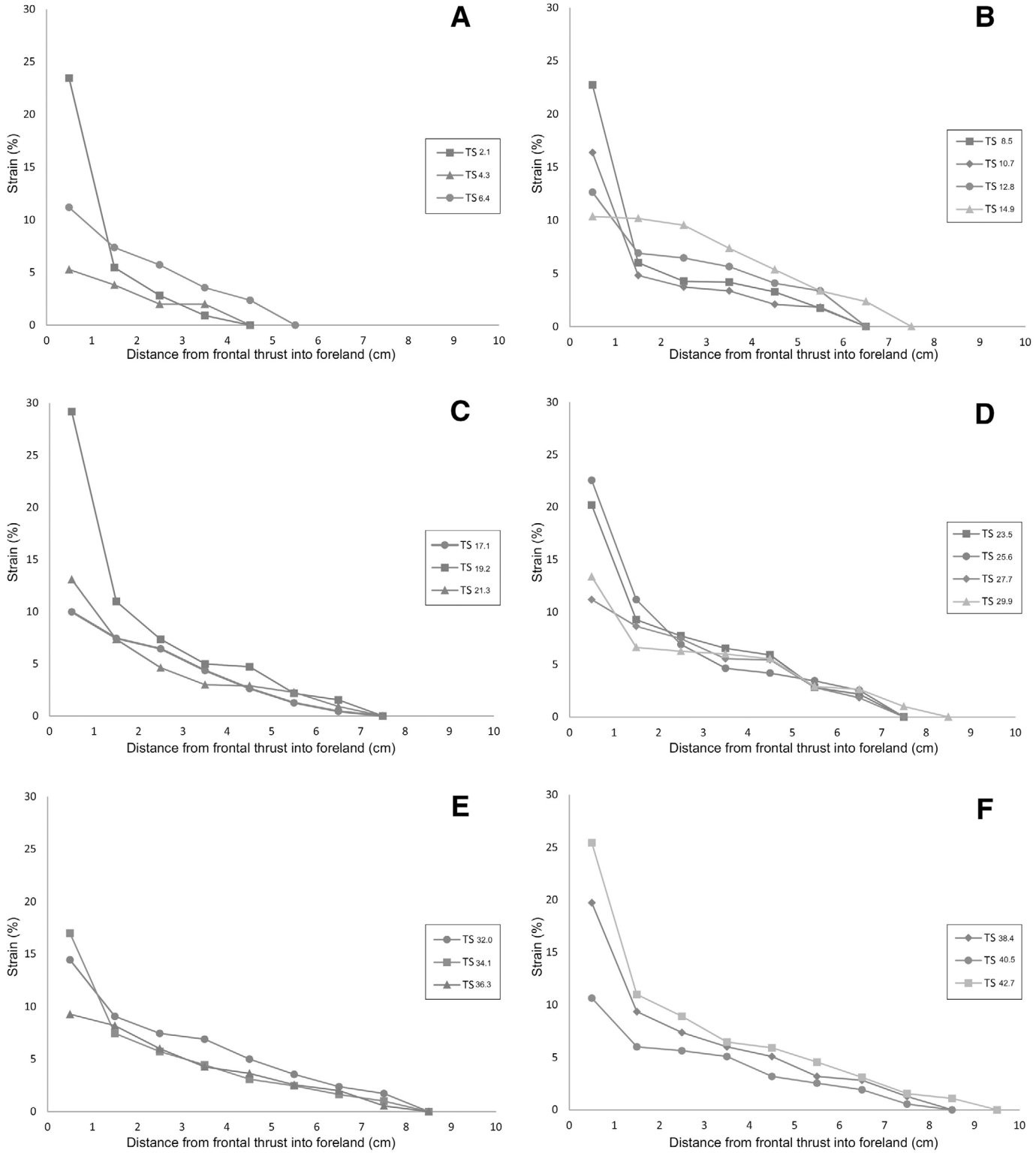

Figure 16. Data from all models illustrating the variation in penetrative strain within this foreland zone for all stages of deformation. (A) Data from shortening amounts 2%–6%. (B) Data from shortening amounts 8%–15%. (C) Data from shortening amounts 17%–21%. (D) Data from shortening amounts 23%–29%. (E) Data from shortening amounts 32%–36%. (F) Data from shortening amounts 38%–42%. All shortening increments show the same exponential decrease as Figure 15. TS—total shortening.

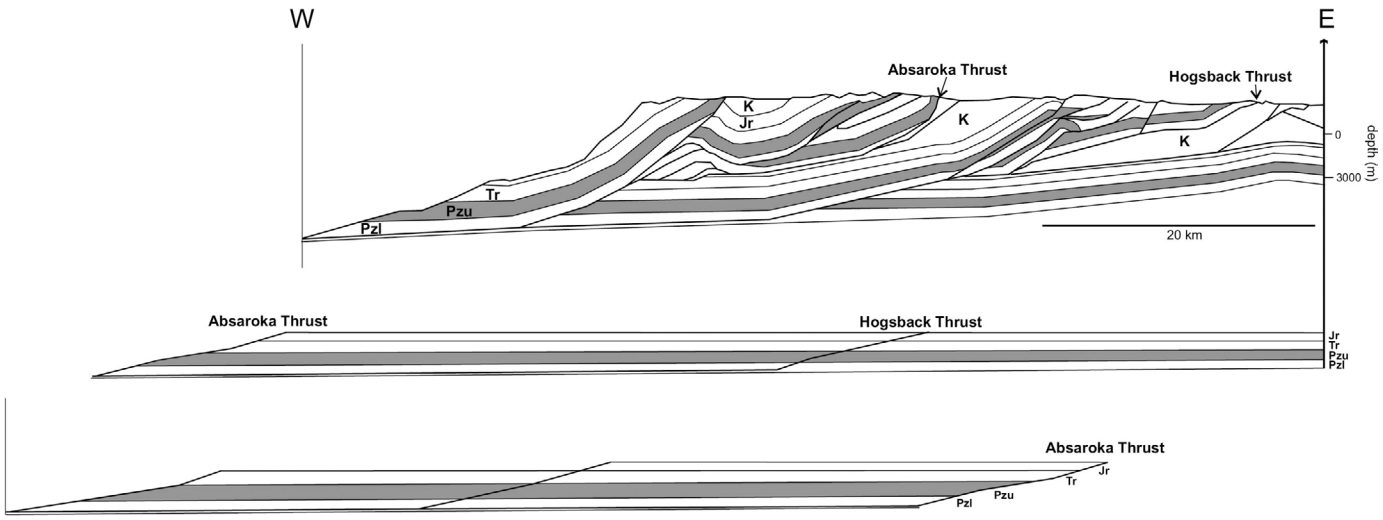

Figure 17. Comparison to an example from the Wyoming salient, after Yonkee and Weil (2010). The upper image shows the segment reproduced from Yonkee and Weil (2010). The lower images show the restored thrust systems. Pzl—Lower Paleozoic units, Pzu—Upper Paleozoic units (shaded gray), Tr—Triassic units, Jr—Jurassic units, and K—Cretaceous units. Important thrust faults are labeled.

Comparison to a Natural Example

The restoration methodology described in Figure 4 and the associated text has also been applied to a cross section of the Wyoming salient, after Yonkee and Weil (2010). The section was chosen as a reasonable analog to the structures created in the models, forming the frontal region of a fold-and-thrust belt. In addition, Mitra (1994), Weil and Yonkee (2009), and Yonkee and Weil (2010) have provided data on the penetrative strain within individual thrust systems, providing an ideal comparison between model results and natural examples. A portion of the original cross section has been digitized (Fig. 17A), covering the Hogsback thrust system and the majority of the Absaroka thrust system. The remainder of the Absaroka system and the hinterland thrust systems have been excluded because of dissimilarity to the models in terms of thrust imbrication or decoupling of the Cretaceous section. The cross-section segment was restored in MOVE, using sequential unfaulting and unfolding algorithms until all deformation was removed. Penetrative strain calculations were carried out using the Triassic red beds as a key unit, in line with the papers cited.

The deformed length of the cross section is 74.9 km, and the restored length is 153.6 km (Fig. 17); thus, there is 78.7 km (51%) of shortening accommodated by folding and thrusting in this section. The closest model for comparison is model 8, where the shortening is 42.7%. By comparison with this model, strain accommodated by folding and thrusting is predicted to be at minimum 88% of the total shortening in the middle parts of the sedimentary sequence, and penetrative strain should account for 12% of the total shortening. Thus, 78.7 km shortening is in fact 88% of the total shortening, indicating that the shortening accommodated by penetrative strain is ~10.7 km. In this fashion, a predicted amount of penetrative strain can be generated from the calculated shortening by folding and thrusting and the model results detailed herein, leading to a more accurate estimate of the total shortening across the region.

Yonkee and Weil (2010) reported ~5% penetrative strain (that is, 3.8 km shortening) for the Hogsback thrust system. Mitra (1994) reported ~15% penetrative strain in the Absaroka thrust system, which is equivalent to ~10 km of shortening across this system. This field data imply that there should be ~13.8 km of shortening across the cross-section segment used in Figure 17. Given the limited mechanisms available for the accommodation of penetrative strain in the models, and the expectation that the model results are minima in terms of expected shortening, the field data are considered to validate the modeling approach and the usefulness of the calculations performed.

Discussion

These results correlate well with the few previous analog modeling studies that have investigated penetrative strain, typically considering the subset of total penetrative strain accommodated by layer-parallel shortening. One such study is by Koyi (1995), which discussed the

behavior of imbricate thrust sheets in a deforming wedge. Penetrative strain dominates the deformation process in the early stages (around 85% of the total shortening in his models compared to 65% in this study) but is less important than deformation accommodated by folding and thrusting in the later stages. Koyi (1995) also noted the increase in layer-parallel shortening with depth noted in this contribution, as did Groshong et al. (2012) and Schlische et al. (2014). The increase of layer-parallel shortening with depth is also predicted by numerical models such as those of Epard and Groshong (1995) and Groshong and Epard (1994) and is seen in the natural examples investigated by Mitra (1994). The general trend of increasing penetrative strain with depth and corresponding decreasing fault slip with depth is apparent from figures in the preceding papers but is not specifically documented. Last, results show that increased total shortening is expected to lead to a decrease in the contribution of the penetrative strain component of the deformation, and this general pattern is replicated between laboratories.

However, this study provides a higher level of detail about penetrative strain amounts within the wedge and into the foreland, related to the growth of the wedge and the initiation of new thrust sheets, than the cited previous analog modeling work. This higher level of detail, and the oscillation in amount of penetrative strain accommodated by the layers between the initiations of successive thrust faults (Fig. 13) may account for the differences in reported magnitudes of penetrative strain in different laboratory models, as results are recorded at different total shortenings calculated over variable starting lengths and including differing amounts of undeformed material (e.g., 50% in Koyi [1995]; 42% in this study; 15% in Groshong et al. [2012] and Schlische et al. [2014]). An additional source of variation is the basal friction, which is higher in this work than in Koyi (1995) due to the use of a plywood base rather than a Plexiglas base. This difference, coupled with the thicker sand pack used in the models discussed here, indicates that the conditions at which the thrust wedge reaches a stable state will vary between laboratories. Since penetrative strain amounts vary as the deforming system tends to or maintains a stable state, the boundary conditions and deformation style must be considered when comparing results. This paper has not reproduced the result of Groshong et al. (2012) of overall dilation within the model rather than overall volume reduction. Minor dilation is noted as the older thrusts are passively rotated within the wedge, which was also noted by Koyi (1995) and Nilforoushan and Koyi (2007). This difference in dilation amount is also attributed to variations in initial configuration and shortening rate, where the models in Groshong et al. (2012) had a thicker initial sand pack and a considerably faster shortening rate.

When comparing model results presented herein and in previous studies with natural examples, it is necessary to remember the limitations of the analog models in replicating the initial conditions in the natural system. These limitations imply that caution should be used extrapolating model results directly to natural situations in the absence of any other constraints on penetrative strain amounts. As discussed in the Materials and Methods section, the mechanism for penetrative strain accommodation in the models is grain-grain displacement, rather than the variety of mechanisms over multiple scales that operate in a natural setting. In this study, the zone where penetrative strain is accommodated in the system appears to migrate, being concentrated in the active thrust, as noted by Koyi et al. (2004), and in a foreland zone that is approximately as wide as the thrust wedge. This may be a natural result of strain saturation within the wedge; i.e., maximum compaction has been achieved in the thrust sheets nearest the backstop, and so compaction (penetrative strain) can only occur to the foreland. In this case, the magnitudes of penetrative strain developed in the models are expected to underestimate the magnitudes of penetrative strain developed in nature. Natural systems may not have a limit to the amount of penetrative strain that can be accommodated by mechanisms such as pressure solution, particularly in the internal portions of the belt; thus, theoretically, a large amount of penetrative strain can be accommodated.

An additional difference between the modeled structures and natural examples concerns the dip and spacing of the modeled thrusts. Modeled thrusts are more closely spaced and dip more steeply than in the Wyoming salient example, as can be seen by comparison of Figures 5–8 and 17. In terms of penetrative strain, the amount of translation on a fault surface versus the internal strain will vary with fault zone weakness (often a function of fault dip). A weak, often shallowly dipping fault will promote translation of the thrust sheet over internal deformation, whereas a stronger, typically steeper fault will promote accommodation of deformation by internal strain (Dahlen, 1990). Another difference is the development of a stable wedge in the final stages of the models, related to wedge behavior in natural situations. Strictly, the wedge developed in the models is not a true critical wedge (sensu Davis et al., 1983) because the basal taper is zero. The modeled wedge is internally imbricated and propagating to the foreland (stage 1 of wedge development sensu DeCelles and Mitra, 1995), but it does not attain the true supercritical, sliding stage. In addition, faults to the rear of the modeled wedge do not appear to reactivate with increased compression, as in natural situations (DeCelles and Mitra, 1995). This

implies that in nature, additional penetrative strain can be accommodated in the hinterland thrust sheets, and again suggests that the models are underestimates of natural penetrative strain.

A final, crucial difference between the models presented here and natural situations is the strong anisotropic layering in fold-and-thrust belts such as the Wyoming salient example presented. The anisotropy of a natural example suggests that penetrative strain will not vary as smoothly with depth as in the models. The models are most applicable to scenarios where there is no roof thrust or detachment of the upper sequence, and the deformation can be approximated as simple slabs moving over a somewhat frictional basal detachment in the external parts of a fold-and-thrust belt rather than the internal portions. The basal friction variability is also likely to affect the distribution of penetrative strain and the tendency for internal strain versus thrust sheet translation, with higher friction promoting higher penetrative strains.

With the data presented in this paper, it has not been possible to document the penetrative strain amounts within individual thrust sheets or individual layers within the thrust sheets, as was done in the studies cited in the "Comparison to a Natural Example" section. While the models are similar enough for the analysis presented here to be undertaken, comparisons of penetrative strain in individual sheets cannot be compared between models because of the subtle variation. Photographs of the side wall of the model cannot be used for this either, as inspection of the map view, side view, and cross-section photographs for a single model suggests that the thrusts visible in the center of the model do not necessarily propagate to the edges or are significantly rotated (due to edge effects), thus introducing an additional source of error. However, even with that caveat, the estimated missing shortening due to penetrative strain from the example shown in Figure 17 is close to the sum of the estimated penetrative strain from the individual sheets from Mitra (1994) and Yonkee and Weil (2010).

Another interesting pattern from certain field data is replicated in these models, suggesting that even if the magnitude of penetrative strain is underestimated due to strain saturation, the models are reproducing a natural phenomenon in the external portions of fold-and-thrust belts. One example is the exponential decay of reported penetrative strain away from the deformation front into the foreland (Fig. 15). This pattern is in good agreement with the results of Craddock and van der Pluijm (1989), who found an exponential decay in layer-parallel shortening recorded by calcite strain fabrics with increasing distance from the Appalachian deformation front into the foreland. This indicates that the distances over which far-field stresses can be experienced during orogenesis extend a considerable distance into the foreland and the craton interior. Thus, despite the assumptions in this model series, the estimated shortening amounts and the general pattern in the distribution of penetrative strain presented herein are considered applicable to natural situations.

Conclusions

Eight analog models run in this study have demonstrated that: (1) penetrative strain is accommodated at every stage of deformation, since a component of penetrative strain was observed in every model; and (2) in early stages of deformation, penetrative strain forms the dominant component of the total shortening, decreasing as the deforming wedge tends to stability and oscillating from higher to lower values as the wedge deforms close to criticality. This oscillation is related to the initiation of thrust faults—penetrative strain increases until a thrust fault develops, abruptly decreases, and then increases again until the next failure point. Also, concerning the distribution of penetrative strain in the system, (3) penetrative strain increases with depth in the sedimentary sequence, is concentrated in the active thrust sheet and a foreland deformation zone, and decays exponentially away from the deformation front in this foreland zone. The same patterns are observed in nature, although the analog models appear to underestimate the strain magnitude due to the differences in the mechanisms by which models and nature accommodate penetrative strain.

Restoration of a cross section across the Wyoming salient, where there are independent measures of the penetrative strain accommodated in certain thrust sheets, indicates that the estimate of the penetrative strain component derived from the models is of the correct order of magnitude. The model estimate appears to be an underestimate, for reasons that have been discussed, but there is clear application of the analog model results to natural examples. Estimates of this type may be made for additional cross sections and may provide answers to the problem of "missing shortening" across orogens and the total amount of shortening experienced at collisional plate margins.

Acknowledgments — This work was supported by a Layman Award from the University of Nebraska–Lincoln. I thank Matty Mookerjee and Sarah Titus for constructive reviews of an earlier version of this manuscript, and I thank Steven Wojtal and Gautam Mitra for constructive reviews on this version. I thank Midland Valley Ltd. For the use of the MOVE software under an academic agreement with the University of Nebraska–Lincoln. I thank Arlo Weil for his constructive editorial comments. Last, I thank Chris Jackson and Bill Dunne for fruitful discussion of the ideas contained in this manuscript.

References Cited

Agard, P., Omrani, J., Jolivet, L., and Moutherea, F., 2005, Convergence history across Zagros (Iran): Constraints from collisional and earlier deformation: International Journal of Earth Sciences, v. 94, p. 401–419, doi:10.1007/s00531-005-0481-4

Beutner, E.C., and Charles, E.G., 1985, Large volume loss during cleavage formation, Hamburg Sequence, Pennsylvania: Geology, v. 13, p. 803–805, doi:10.1130/0091-7613(1985)13<803:LVLDCF>2.0.CO;2

Buiter, S.J.H., 2012, A review of brittle compressional wedge models: Tectonophysics, v. 530–531, p. 1–17, doi: 10.1016/j.tecto.2011.12.018

Couzens, B.A., Dunne, W.M., Onasch, C.M., and Glass, R., 1993, Strain variations and three-dimensional strain factorization at the transition from the southern to the central Appalachians: Journal of Structural Geology, v. 15, no. 3–5, p. 451–464, doi:10.1016/0191-8141(93)90140-6

Couzens-Schultz, B.A., Vendeville, B.C., and Wiltschko, D.V., 2003, Duplex style and triangle zone formation: Insights from physical modeling: Journal of Structural Geology, v. 25, p. 1623–1644, doi:10.1016/S0191-8141(03)00004-X

Craddock, J.P., and van der Pluijm, B.A., 1989, Late Paleozoic deformation of the cratonic carbonate cover of eastern North America: Geology, v. 17, p. 416–419, doi: 10.1130/0091-7613(1989)017<0416:LPDOTC>2.3.CO;2

Dahlen, F.A., 1990 Critical taper model of fold-and-thrust belts and accretionary wedges: Annual Review of Earth and Planetary Sciences, v. 18, p. 55–99, doi:10.1146/annurev.ea.18.050190.000415

Davis, D., Suppe, J., and Dahlen, F., 1983, Mechanics of foldand- thrust belts and accretionary wedges: Journal of Geophysical Research, v. 88, no. B2, p. 1153–1172, doi: 10.1029/JB088iB02p01153

Dean, S.L., Kulander, B.R., and Skinner, J.M., 1988, Structural chronology of the Alleghanian orogeny in southeastern West Virginia: Geological Society of America Bulletin, v. 100, p. 299–310, doi:10.1130/0016-7606(1988)100<0299:SCOTAO>2.3.CO;2

DeCelles, P.G., and Mitra, G., 1995, History of the Sevier orogenic wedge in terms of critical taper models, northeast Utah and southwest Wyoming: Geological Society of America Bulletin, v. 107, no. 4, p. 454–462, doi: 10.1130/0016 -7606(1995)107<0454:HOTSOW>2.3.CO;2

Ellis, S., Schreurs, G., and Panien, M., 2004, Comparisons between analogue and numerical models of thrust wedge development: Journal of Structural Geology, v. 26, p. 1659–1675, doi:10.1016/j.jsg.2004.02.012

Engelder, T., 1979, Mechanisms for strain within the Upper Devonian clastic sequence of the Appalachian Plateau, western New York: American Journal of Science, v. 279, p. 527–542, doi:10.2475/ajs.279.5.527

Engelder, T., and Engelder, R., 1977, Fossil distortion and decollement tectonics of the Appalachian Plateau: Geology, v. 5, p. 457–460, doi:10.1130/0091-7613(1977)5<457:FDADTO>2.0.CO;2

Epard, J.-L., and Groshong, R.H., Jr., 1995, Kinematic model of detachment folding including limb rotation, fixed hinges and layer-parallel strain: Tectonophysics, v. 247, p. 85–103, doi:10.1016/0040-1951(94)00266-C

Fischer, M.W., and Coward, M.P., 1982, Strains and folds within thrust sheets: The Heilam sheet, NW Scotland: Tectonophysics, v. 88, p. 291–312, doi: 10.1016/0040-1951(82)90241-4

Fisher, D., 1990, Orientation history and rheology in slates, Kodiak and Afognak Islands, Alaska: Journal of Structural Geology, v. 12, no. 4, p. 483–498, doi: 10.1016 /0191-8141(90)90036-X

Geiser, P., and Engelder, T., 1983, The distribution of layer parallel shortening fabrics in the Appalachian foreland of New York and Pennsylvania: Evidence for two noncoaxial phases of the Alleghanian orogeny, *in* Hatcher, R.D., Jr., Williams, H., and Zietz, I., eds., Contributions to the Tectonics and Geophysics of Mountain Chains: Geological Society of America Memoir 158, p. 161–176, doi: 10.1130/MEM158-p161

Gray, M.B., and Mitra, G., 1993, Migration of deformation fronts during progressive deformation: Evidence from detailed structural studies in the Pennsylvania Anthracite Region, USA: Journal of Structural Geology, v. 15, p. 435–449, doi:10.1016/0191-8141(93)90139-2\

Groshong, R.H., Jr., 1975, Strain, fractures and pressure solution in natural single-layer folds: Geological Society of America Bulletin, v. 86, p. 1363–1376, doi:10.1130/0016-7606(1975)86<1363:SFAPSI>2.0.CO;2

Groshong, R.H., Jr., and Epard, J.-L., 1994, The role of strain in area-constant detachment folding: Journal of Structural Geology, v. 16, p. 613–618, doi:10.1016/0191-8141(94)90113-9.

Groshong, R.H., Jr., Withjack, M.O., Schlische, R.W., and Hidayah, T.N., 2012, Bed length does not remain constant during deformation: Recognition and why it matters: Journal of Structural Geology, v. 41, p. 86–97, doi: 10.1016/j.jsg.2012.02.009

Guest, B., Axen, G.J., Lam, P.S., and Hassanzadeh, J., 2006, Late Cenozoic shortening in the west central Alborz Mountains, northern Iran, by combined conjugate strike-slip and thin-skinned deformation: Geosphere, v. 2, p. 35–52, doi:10.1130/GES00019.1

Guillot, S., Garzanti, E., Baratoux, D., Marquer, D., Maheo, G., and de Sigoyer, J., 2003, Reconstructing the total shortening history of the NW Himalaya: Geochemistry Geophysics Geosystems, v. 4, no. 7, doi: 10.1029/2002GC000484

Henderson, J.R., Wright, T.O., and Henderson, M.N., 1986, A history of cleavage and folding: An example from the Goldenville Formation, Nova Scotia: Geological Society of America Bulletin, v. 97, p. 1354–1366, doi:10.1130/0016-7606(1986)97<1354:AHOCAF>2.0.CO;2

Hessami, K., Nilforoushan, F., and Talbot, C.J., 2006, Active deformation within the Zagros Mountains deduced from GPS measurements: Journal of the Geological Society of London, v. 163, p. 143–148, doi:10.1144/0016-764905-031

Hogan, J.P., and Dunne, W.M., 2001, Calculation of shortening due to outcrop-scale deformation and its relation to regional deformation patterns: Journal of Structural Geology, v. 23, p. 1507–1529, doi:10.1016/S0191-8141(01)00016-5

Hubbert, M.K., 1937, Theory of scale models as applied to the study of geologic structures: Geological Society of America Bulletin, v. 48, p. 1459–1520, doi:10.1130/GSAB-48-1459

Jaeger, J.C., Cook, N.G.W., and Zimmerman, R.W., 2007, Fundamentals of Rock Mechanics (4th ed.): Malden, Massachusetts and Oxford, UK, Blackwell Publishing, 475 p.

Johnson, M.R.W., 2002, Shortening budgets and the role of continental subduction during the India–Asia collision: Earth-Science Reviews, v. 59, no. 1–4, p. 101–123, doi: 10.1016/S0012-8252(02)00071-5

Koyi, H.A., 1995, Mode of internal deformation in sand wedges: Journal of Structural Geology, v. 17, p. 293–300, doi:10.1016/0191-8141(94)00050-A

Koyi, H.A., 1997, Analogue modelling: From a qualitative to a quantitative technique—A historical outline: Journal of Petroleum Geology, v. 20, no. 2, p. 223–238, doi: 10.1111 /j.1747-5457.1997.tb00774.x

Koyi, H.A., and Vendeville, B.C., 2003, The effect of decollement dip on geometry and kinematics of model accretionary wedges: Journal of Structural Geology, v. 25, p. 1445–1450, doi:10.1016/S0191-8141(02)00202-X

Koyi, H.A., Sans, M., Teixell, A., Cotton, J., and Zeyen, H., 2004, The significance of penetrative strain in the restoration of shortened layers—Insights from sand models and the Spanish Pyrenees, *in*

McClay, K.R., ed., Thrust Tectonics and Hydrocarbon Systems: American Association of Petroleum Geologists Memoir 82, p. 207–222.

Krantz, R.W., 1991, Measurements of friction coefficients and cohesion for faulting and fault reactivation in laboratory models using sand and sand mixtures: Tectonophysics, v. 188, p. 203–207, doi:10.1016/0040-1951(91)90323-K

Kwon, S., and Mitra, G., 2004, Strain distribution, strain history and kinematic evolution associated with the formation of arcuate salients in fold-thrust belts: The example of the Provo salient, Sevier orogeny, Utah, *in* Sussman, A.J., and Weil, A.B., eds., Orogenic Curvature: Integrating Paleomagnetic and Structural Analyses: Geological Society of America Special Paper 383, p. 205–223, doi: 10.1130/0-8137-2383-3(2004)383[205:SDSHAK]2.0.CO;2

Li, C., Prikryl, R., and Nordlund, E., 1998, The stress-strain behavior of rock material related to fracture under compression: Engineering Geology, v. 49, p. 293–302, doi: 10.1016 /S0013-7952(97)00061-6

Lohrmann, J., Kukowski, N., Adam, J., and Oncken, O., 2003, The impact of analogue material properties on the geometry, kinematics and dynamics of convergent sand wedges: Journal of Structural Geology, v. 25, p. 1691–1711, doi:10.1016/S0191-8141(03)00005-1

Mitra, G., 1994, Strain variation in thrust sheets across the Seviers fold-and-thrust belt (Idaho-Utah-Wyoming): Implications for section restoration and wedge taper evolution: Journal of Structural Geology, v. 16, no. 4, p. 585–602, doi:10.1016/0191-8141(94)90099-X

Mitra, G., and Yonkee, W.A., 1985, Relationship of spaced cleavage to folds and thrusts in the Idaho-Utah-Wyoming thrust belt: Journal of Structural Geology, v. 7, no. 3/4, p. 361–373, doi:10.1016/0191-8141(85)90041-0

Mitra, G., Yonkee, W.A., and Gentry, D.J., 1984, Solution cleavage and its relationship to major structures in the Idaho-Utah-Wyoming thrust belt: Geology, v. 12, p. 354–358, doi:10.1130/0091-7613(1984)12<354:SCAIRT>2.0.CO;2

Moretti, I., and Callot, J.-P., 2012, Area, length and thickness conservation: Dogma or reality?: Journal of Structural Geology, v. 41, p. 64–75, doi:10.1016/j.jsg.2012.02.014

Mouthereau, F., Lacombe, O., and Verges, J., 2012, Building the Zagros collisional orogen: Timing, strain distribution and the dynamics of Arabia/Eurasia plate convergence: Tectonophysics, v. 532–535, p. 27–60, doi: 10.1016/j.tecto.2012.01.022

Nilforoushan, F., and Koyi, H.A., 2007, Displacement fields and finite strains in a sandbox model simulating a foldthrust belt: Geophysical Journal International, v. 169, p. 1341–1355, doi:10.1111/j.1365-246X.2007.03341.x

Nilforoushan, F., Masson, P., Vernant, P., Vigny, C., Martinod, J., Abbassi, M., Nankali, H., Hatzfeld, D., Bayer, R., Tavakoli, F., Ashtiani, A., Doerflinger, E., Daignières, M., Collard, P., and Chéry, J., 2003, GPS network monitors the Arabia-Eurasia collision deformation in Iran: Journal of Geodesy, v. 77, p. 411–422, doi:10.1007/s00190-003-0326-5

Onasch, C.M., 1993, Determination of pressure solution shortening in sandstones: Tectonophysics, v. 227, p. 145–159, doi:10.1016/0040-1951(93)90092-X

Panien, M., Schreurs, G., and Pfiffner, A., 2006, Mechanical behaviour of granular materials used in analogue modelling: Insights from grain characterization, ring-shear tests and analogue experiments: Journal of Structural Geology, v. 28, p. 1710–1724, doi:10.1016/j.jsg.2006.05.004

Sans, M., Verges, J., Gomis, E., Pares, J.M., Schiattarella, M., Trave, A., Calvet, F., Santanach, P., and Doulcet, A., 2003, Layer parallel shortening in salt-detached folds: Constraint on cross-section restoration: Tectonophysics, v. 372, p. 85–104, doi:10.1016/S0040-1951(03)00233-6

Schellart, W., 2000, Shear test results for cohesion and friction coefficients for different granular materials: Scaling implications for their usage in analogue modelling: Tectonophysics, v. 324, p. 1–16, doi:10.1016/S0040-1951(00)00111-6

Schlische, R.W., Groshong, R.H., Jr., Withjack, M., and Hidayah, T.N., 2014, Quantifying the geometry, displacements and subresolution deformation in thrust-ramp anticlines with growth and erosion: From models to seismic-reflection profile: Journal of Structural Geology, v. 69, p. 304–319, doi:10.1016/j.jsg.2014.07.012

Sussman, A.J., Pueyo, E.L., Chase, C.G., Mitra, G., and Weil, A.B., 2012, The impact of vertical-axis rotations on shortening estimates: Lithosphere, v. 4, no. 5, p. 383–394, doi:10.1130/L177.1

Tapp, B., and Wickham, J., 1987, Relationships of rock cleavage fabrics to incremental and accumulated strain in the Conococheague Formation, USA: Journal of Structural Geology, v. 9, no. 4, p. 457–472, doi:10.1016/0191-8141(87)90121-0

Tavarnelli, E., 1997, Structural evolution of a foreland foldthrust belt: The Umbria-Marche Apennines, Italy: Journal of Structural Geology, v. 19, p. 523–534, doi:10.1016/S0191-8141(96)00093-4

Vernant, P., Fadil, A., Mourabit, T., Ouazar, D., Koulali, A., Davila, J.M., Garate, J., McClusky, S., and Reilinger, R., 2010, Geodetic constraints on active tectonics of the Western Mediterranean: Implications for the kinematics and dynamics of the Nubia-Eurasia plate boundary zone: Journal of Geodynamics, v. 49, p. 123–129, doi: 10.1016/j.jog.2009.10.007

Weil, A.B., and Yonkee, A., 2009, Anisotropy of magnetic susceptibility in weakly deformed red beds from the Wyoming salient, Sevier thrust belt: Relations to layerparallel shortening and orogenic curvature: Lithosphere, v. 1, no. 4, p. 235–256, doi:10.1130/L42.1

Weil, A.B., Yonkee, A., and Sussman, A., 2010, Reconstructing the kinematic evolution of curved mountain belts: A paleomagnetic study of Triassic red beds from the Wyoming salient, Sevier thrust belt, USA: Geological Society of America Bulletin, v. 122, no. 1–2, p. 3–23, doi: 10.1130 /B26483.1

Whitaker, A.E., and Bartholomew, M.J., 1999, Layer parallel shortening: A mechanism for determining deformation timing at the junction of the Central and Southern Appalachians: American Journal of Science, v. 299, p. 238–254, doi:10.2475/ajs.299.3.238

Wiltschko, D.V., Medwedeff, D.A., and Millson, H.E., 1985, Distribution and mechanisms of strain within rocks on the northwest ramp of Pine Mountain block, Southern Appalachian foreland: A field test of theory: Geological Society of America Bulletin, v. 96, p. 426–435, doi: 10.1130/0016-7606(1985)96<426:DAMOSW>2.0.CO;2

Wojtal, S., 1989, Measuring displacement gradients and strains in faulted rocks: Journal of Structural Geology, v. 11, no. 6, p. 669–678, doi:10.1016/0191-8141 (89) 90003-5.

Yonkee, A., and Weil, A.B., 2010, Reconstructing the kinematic evolution of curved mountain belts: Internal strain patterns in the Wyoming salient, Sevier thrust belt, USA: Geological Society of America Bulletin, v. 122, no. 1–2, p. 24–49, doi:10.1130/B26484.1

Zhao, W., Nelson, K.D., and Project INDEPTH Team, 1993, Deep seismic reflection evidence for continental underthrusting beneath south Tibet: Nature, v. 366, p. 557–559, doi:10.1038/366557a0.